JACS
JOURNAL OF THE AMERICAN CHEMICAL SOCIETY
Article
Cite This: J. Am. Chem. Soc. 2019, 141, 18994−19001
pubs.acs.org/JACS

Direct Observation of Symmetry-Dependent Electron−Phonon Coupling in Black Phosphorus

Nannan Mao,[†,‡,∥] Xingzhi Wang,[‡,§,∥] Yuxuan Lin,[†] Bobby G. Sumpter,[⊥,#] Qingqing Ji,[†] Tomás Palacios,[†] Shengxi Huang,[○] Vincent Meunier,[▽] Mildred S. Dresselhaus,[†] William A. Tisdale,[◇] Liangbo Liang,[*,⊥] Xi Ling,[*,‡,§,¶] and Jing Kong[*,†]

[†]Department of Electrical Engineering and Computer Science and [◇]Department of Chemical Engineering, Massachusetts Institute of Technology, Cambridge, Massachusetts 02139, United States

[‡]Department of Chemistry and [§]Division of Materials Science and Engineering, [¶]The Photonics Center, Boston University, Boston, Massachusetts 02215, United States

[⊥]Center for Nanophase Materials Sciences and [#]Computational Sciences and Engineering Division, Oak Ridge National Laboratory, Oak Ridge, Tennessee 37831, United States

[○]Department of Electrical Engineering, The Pennsylvania State University, University Park, Pennsylvania 16802, United States

[▽]Department of Physics, Applied Physics, and Astronomy, Rensselaer Polytechnic Institute, Troy, New York 12180, United States

Supporting Information

ABSTRACT: Electron−phonon coupling in two-dimensional nanomaterials plays a fundamental role in determining their physical properties. Such interplay is particularly intriguing in semiconducting black phosphorus (BP) due to the highly anisotropic nature of its electronic structure and phonon dispersions. Here we report the direct observation of symmetry-dependent electron−phonon coupling in BP by performing the polarization-selective resonance Raman measurement in the visible and ultraviolet regimes, focusing on the out-of-plane A_g^1 and in-plane A_g^2 phonon modes. Their intrinsic resonance Raman excitation profiles (REPs) were extracted and quantitatively compared. The in-plane A_g^2 mode exhibits remarkably strong resonance enhancement across the excitation wavelengths when the excitation polarization is parallel to the armchair (A_g^2//AC) direction. In contrast, a dramatically weak resonance effect was observed for the same mode with the polarization parallel to zigzag (A_g^2//ZZ) direction and for the out-of-plane A_g^1 mode (A_g^1//AC and A_g^1//ZZ). Analysis on quantum perturbation theory and first-principles calculations on the anisotropic electron distributions in BP demonstrated that electron−phonon coupling considering the symmetry of the involved excited states and phonon vibration patterns is responsible for this phenomenon. Further analysis of the polarization-dependent REPs for A_g phonons allows us to resolve the existing controversies on the physical origin of Raman anomaly in BP and its dependence on excitation energy, sample thickness, phonon modes, and crystalline orientation. Our study gives deep insights into the underlying interplay between electrons and phonons in BP and paves the way for manipulating the electron−phonon coupling in anisotropic nanomaterials for future device applications.

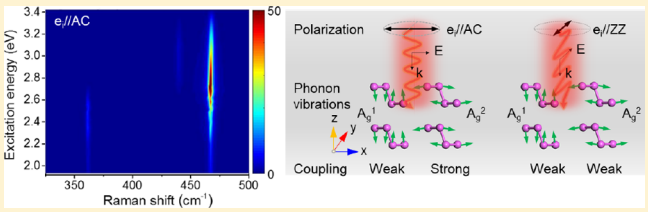

INTRODUCTION

The interaction of electrons with lattice vibrations in solids plays an important role for a variety of physical phenomena, including Raman scattering, electronic and thermal transport, and superconductivity. Resonance Raman scattering, which involves the interplay of electrons, photons, and phonons over a broad range of excitation energy, has been widely used to study the interband electronic transitions and excitons as well as their interactions with phonons in two-dimensional (2D) crystals.[1−8] For instance, it can provide rich information on the interlayer and intralayer electron−phonon interaction in twisted graphene heterostructures[2] and the coupling of quasiparticle states (such as excitons, trions, and dark excitons) with phonons in transition metal dichalcogenides.[4−6,9] Moreover, since the electron−phonon coupling involved in a Raman scattering event is strictly governed by the symmetry of the phonon modes and the corresponding excited state, resonance Raman scattering is also a powerful way to provide deep insights into symmetry-dependent electron−phonon coupling,[5,10] which is critical for low-symmetry 2D crystals such as black phosphorus (BP) and rhenium disulfide (ReS_2).

BP is a representative low-symmetry semiconductor with an orthorhombic crystal structure that has attracted intense attention since its 2D realizations manifest many outstanding properties, including a thickness-tunable direct band gap from the visible to the mid-infrared region, strongly bound excitons

Received: August 1, 2019
Published: November 5, 2019

DOI: 10.1021/jacs.9b07974
J. Am. Chem. Soc. 2019, 141, 18994−19001

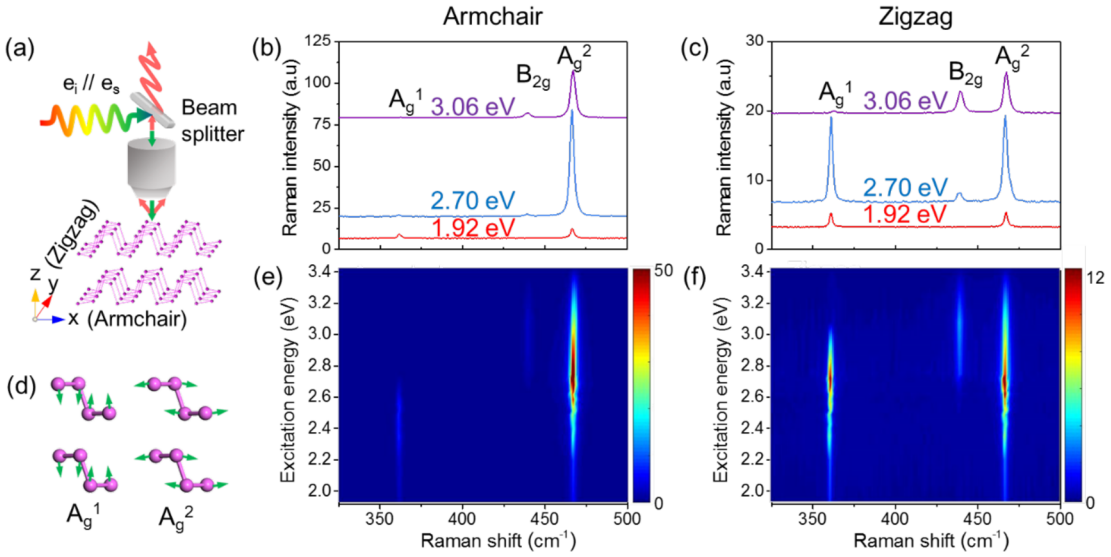

Figure 1. Schematic illustration of the Raman experiments and excitation-energy-dependent polarized Raman spectra of BP. (a) Schematic illustration of the polarized Raman configuration. e_i and e_s represent the polarizations of the incident and scattering light, respectively. x and y axes are the AC and ZZ directions of BP, respectively. (b and c) Normalized polarized Raman spectra of a 7.7 nm thick BP with excitation energies at 1.92, 2.70, and 3.06 eV with P//AC (b) and P//ZZ (b). (d) Corresponding lattice vibration patterns of A_g^1 and A_g^2 phonon modes in BP. (e and f) Intensity maps of the excitation-energy-dependent polarized Raman spectra of BP with P//AC (e) and P//ZZ (f). Interpolation was used in e and f for clear presentation of the resonant energy region. Raman intensities in b, c, e, and f have been normalized to the Raman peak of a single-crystal quartz at 465 cm^{-1}.

and trions, and an in-plane anisotropy, which are all promising traits for electronic and optoelectronic applications.[11−18] In particular, BP's puckered atomic structure endows it with anisotropic electronic structure. This leads to anisotropic electron−photon and electron−phonon interactions, which play a key role in its anisotropic optical, electronic, and thermal properties.[13,17,19,20] The anisotropic electron−photon coupling, evidenced by a linear dichroism in the visible and IR regime as well as anisotropic exciton and trion effect, has been intensely investigated in BP.[13,15−18,21] However, the electron−phonon coupling in BP is not fully understood due to the complexity of both the highly anisotropic electronic and the phonon behaviors. The complexity is evidenced by the intricate anisotropic Raman scattering in BP, which has caused great controversy among different groups regarding its physical origin during the past few years.[19,22−27] Previous studies demonstrated that the excitation energy, the thickness of BP and the symmetry of phonon modes all contribute to the complexity of its polarized Raman spectra.[19,22−26,28] Despite many attempts to understand this unusual phenomenon, most of them only took into account the apparent anisotropic electron−photon coupling, leaving the electron−phonon coupling ignored.[19,22,23,25,28] Therefore, a systematic study focusing on the electron−phonon coupling is highly desirable to reveal the underlying physical origin of the complex anisotropic Raman scattering in BP and other similar low-symmetry crystals.

Herein, we report direct evidence of symmetry-dependent electron−phonon coupling for A_g phonons in BP by performing polarization- and excitation-energy-dependent Raman measurements from the visible to the ultraviolet (UV) regime. The in-plane A_g^2 mode shows a significantly stronger resonance effect across the excitation wavelengths when the laser polarization is parallel to the armchair direction (A_g^2//AC) of BP than that along the zigzag direction (A_g^2//ZZ), suggesting much stronger electron−phonon coupling. In contrast, we observe comparatively weak electron−phonon coupling for the out-of-plane A_g^1 mode (A_g^1//AC and A_g^1//ZZ). Supported by density functional theory (DFT) calculations of the resonance Raman profiles, these features can be understood by quantum perturbation theory considering the match between the symmetries of the related excited states and the phonon vibration patterns. Further analysis of electron−phonon coupling in BP leads to a comprehensive understanding on the physical origin of the intricate anisotropic Raman scattering in BP and its dependence on the excitation energy, sample thickness, and vibration patterns of the phonon modes. This allows us to resolve the existing controversies on the physical origin of the intricate anisotropic Raman scattering of BP and Raman identification of BP's crystalline orientations.

EXPERIMENTAL SECTION

Sample Preparation and Characterization. BP flakes were prepared on fused silica substrates through mechanical exfoliation from the bulk BP crystal (Smart-elements). Their thicknesses were determined by atomic force microscopy (AFM, Veeco Dimension 3100). To prevent degradation of BP samples in ambient conditions, a thin poly(methyl-methacrylate) (PMMA) film was spin coated on top of BP immediately after the AFM experiments.

Raman Measurements. Raman spectra of BP samples with visible excitation wavelengths were measured in a backscattering geometry using a triple-grating Raman system (Horiba JY T64000) equipped with 14 different laser lines (Ar/Kr, Coherent Innova 70C) from 454 to 648 nm. The incident laser was initially horizontally polarized. A 100× objective and an 1800 g/mm grating were used to collect and disperse the Raman signals. Raman spectra excited with ultraviolet (UV) lasers at 364 and 405 nm were collected on a separate Raman system (Horiba HR Evolution). A 100× objective and a deep UV-optimized 40× objective were used to collect the UV Raman signals for 405 and 364 nm excitations, respectively. The laser power was kept below 0.25 mW for high-energy excitations (364 to 568 nm) and 0.56 mW for the 648 nm excitation line. All of the Raman spectra were collected under a parallel configuration, where

DOI: 10.1021/jacs.9b07974
J. Am. Chem. Soc. 2019, 141, 18994−19001

the incident laser polarization is parallel to the scattered laser polarization. BP samples were rotated to change the relative angle between the crystalline orientation and the laser polarization. All of the Raman spectra shown in this work were calibrated by the Raman peak of a single-crystal quartz at 465 cm^{-1} to exclude the unequal influence of the instrumental response to different excitation wavelengths.

RESULTS AND DISCUSSION

Excitation-Energy-Dependent Polarized Raman Spectra in BP. As shown in Figure 1a, the Raman spectra of the exfoliated BP samples were collected on a polarized Raman spectrometer under the parallel polarization configuration. The crystalline orientations of BP were determined by the angle-dependent Raman frequencies of the three phonon modes, A_g^1 (363 cm^{-1}), B_{2g} (440 cm^{-1}), and A_g^2 (467 cm^{-1}).[29] For example, for the BP sample in Figure S1a, its Raman spectra show a slight red shift when the excitation polarization is parallel to the AC direction (P//AC) compared to that with laser polarization along the ZZ direction (P//ZZ) (Figure S1b). Both the Raman intensity and the Raman frequency of A_g^2 for this sample (Figure S1c and S1d) vary periodically with the sample rotation angle when the power of the excitation laser at 2.18 eV is relatively high (1.25 mW). The A_g^2 mode shows the lowest frequency when P//AC, due to larger heating effect induced by the stronger absorption (Figure S1b and S1d).[29] Figure 1b and 1c shows the representative polarized Raman spectra of a 7.7 nm BP flake (~14 layers) under visible (1.92 and 2.70 eV) and UV (3.06 eV) excitation with P//AC and P//ZZ, respectively. Most of them are dominated by two Raman peaks, A_g^1 and A_g^2, as the B_{2g} mode is symmetry forbidden in such a polarization configuration.[19,22−24] A very weak signal of the B_{2g} mode can be observed at higher excitation energy, which is discussed in the Supporting Information. The corresponding lattice vibrations of A_g^1 and A_g^2 phonon modes are shown in Figure 1d. We observed that their Raman intensities depend strongly on the excitation energy and crystalline orientation (Figure 1b and 1c).

Although previous studies have reported that the Raman intensities of BP are dependent on the excitation wavelength, the evolution of the Raman intensities of A_g^1 and A_g^2 modes in a broad range of excitation energy has not been reported.[19,22,23,25] Here, using 16 excitation laser lines covering the visible and UV regimes (1.92−3.41 eV), we are able to obtain the excitation-energy-dependent Raman spectra for BP with different thicknesses. Figure 1e and 1f shows the intensity maps of the normalized excitation-energy-dependent Raman spectra of the 7.7 nm BP with P//AC and P//ZZ, respectively. The corresponding series of Raman spectra under different excitation energies can be found in Figure S2a and S2b. Here we define A_g^1//AC, A_g^2//AC, A_g^1//ZZ, and A_g^2//ZZ as the A_g^1 and A_g^2 Raman peaks measured with the laser polarization along the AC and ZZ directions, respectively. For the 7.7 nm BP it is clear that the intensity of A_g^1//AC is slightly weaker than that of A_g^2//AC when the excitation energy is below 2.2 eV (Figures 1e and S2a). As the excitation energy increases further from 2.2 to 2.5 eV, the intensities of both A_g^1 and A_g^2 modes increase; however, the intensity of the A_g^2 mode increases much faster than that of the A_g^1 mode, leading to much stronger intensity of A_g^2//AC than that of A_g^1//AC. When the excitation energy is above 2.60 eV, the intensity of A_g^1//AC starts to decrease while the intensity of A_g^2//AC keeps increasing. Of particular note, A_g^1 becomes too weak to be noticeable when the excitation energy is above 2.66 eV (Figures 1e and S2a). It is obvious that the A_g^1 and A_g^2 phonons show distinct resonance windows. The A_g^1 phonon shows a weak resonance effect with a resonance window in lower excitation energy (around 2.4 eV), while the A_g^2 phonon has the strongest resonance around 2.71 eV. However, when P//ZZ, the A_g^1 phonon always shows the same level of intensity as the A_g^2 phonon under visible excitations (1.92−2.73 eV). Consequently, A_g^1//ZZ and A_g^2//ZZ show a similar resonance window in the visible region (Figures 1f and S2b).

Intrinsic Raman Excitation Profiles. The normalized Raman intensities of the A_g^1 and A_g^2 phonons as a function of the excitation energy, called Raman excitation profiles (REPs), are depicted for the 7.7 nm BP with P//AC and P//ZZ in Figure 2a. Compared to the other three REPs, the A_g^2//AC profile shows the strongest resonance effect across the entire excitation window. Moreover, these two phonons exhibit different resonance windows when P//AC. Specifically, A_g^1//AC shows the weak resonance effect between 2.20 and 2.60 eV, while the largest resonance effect of A_g^2//AC occurs at higher excitation energy around 2.71 eV. On the contrary, their REPs with P//ZZ are similar in the entire visible region but slightly different in the UV region. For example, the A_g^1 phonon is much weaker than the A_g^2 phonon at 3.04 eV excitation (Figure 2a).

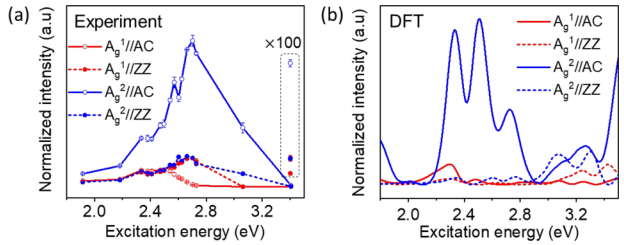

Figure 2. Experimental and theoretical Raman excitation profiles of BP. Experimental (a) and DFT-calculated (b) Raman excitation profiles of A_g^1 (red lines) and A_g^2 (blue lines) with P//AC (solid lines) and P//ZZ (dashed lines) directions. (Inset a) Corresponding Raman intensity at 3.41 eV excitation energy, multiplied by a factor of 100. Note that the excitation energy in b is multiplied by a scaling factor of 1.19 to account for underestimation of energy separations between the valence and the conduction states in DFT calculations.

Surprisingly, when the excitation energy is between 2.60 and 2.73 eV, the A_g^1 mode shows stronger resonance when P//ZZ than that when P//AC. This is an unexpected result since the optical absorption of BP is much larger for P//AC than that for P//ZZ in this excitation energy range.[13,17,19,21] This result implies that other factors, such as the electron−phonon coupling, are more important contributors to the Raman intensity than the intrinsic resonance in this excitation range.

Note that optical interference can also affect the REPs of BP;[19,22] thus, to rule out this extrinsic effect, we calculated the interference enhancement factor of the A_g modes in BP with different thicknesses on a fused silica substrate (details can be found in the Supporting Information). As shown in Figure S3a, the interference enhancement factor for BP is larger for P//ZZ than that for P//AC in the visible region, which is consistent with previous reports.[19,22] For BP with a thickness as thin as 7.7 nm, the calculated enhancement ratio (ZZ/AC) does not vary dramatically with the excitation energy (Figure S3b). Therefore, we conclude that the interference effect does not have a major influence on REPs of the A_g phonon modes for

DOI: 10.1021/jacs.9b07974
J. Am. Chem. Soc. 2019, 141, 18994−19001

this thin sample. However, as the thickness of BP increases to tens of nanometers (15.0−73.0 nm), the influence of the interference effect on the REPs should not be ignored (Figure S4a−f). For instance, the calculated interference enhancement factors of the BP samples with thicknesses of 56.2 and 61.2 nm show a strong peak around 2.60 eV when P//ZZ (Figure S4d and S4e), which will enhance the Raman intensity of A_g^2//ZZ at 2.60 eV strongly, as comparable to that of A_g^2//AC. As shown in Figure S5a and S5b, the measured REPs of A_g^1//ZZ and A_g^2//ZZ of the corresponding BP samples indeed show an obvious resonance peak at 2.60 eV. After calibration with the anisotropic interference effect, the REPs of A_g^1 and A_g^2 for these BP samples and even thicker samples are similar to that of 7.7 (Figure 2a) and 15.0 nm BP (Figure S5c−f), thus reflecting the intrinsic resonance effect in BP.

To corroborate the distinct resonant behaviors of the A_g phonons with P//AC and P//ZZ directions, their Raman intensities in bulk BP were calculated as a function of the laser excitation energy based on first-principles DFT (Figure 2b, details can be found in the Supporting Information). Here the laser excitation energy of BP in DFT was multiplied by a scaling factor of 1.19, because DFT is well known to underestimate the energy separations between the valence and the conduction electronic states, including the band gap.[13,30] The theoretical REPs of both A_g^1 and A_g^2 phonons in Figure 2b are generally consistent with the experimental results shown in Figure 2a. In particular, the calculated results confirm that A_g^2//AC exhibits the strongest resonance effect, especially in the visible region, whereas in the UV region, the differences between the four REPs are reduced. Furthermore, the calculated REPs of A_g^1//AC and A_g^2//AC indeed show very different trends. In contrast, the calculated REPs of A_g^1//ZZ and A_g^2//ZZ show similar trends in the visible region, but their difference increases in the UV region. In short, both the experimental and the theoretical results confirm that the electron−phonon coupling in BP depends on both the vibrational modes and the excitation energy.

Symmetry-Dependent Electron−Phonon Coupling in BP. The origin of the different resonance profiles of the two A_g modes can be understood by an analysis based on quantum perturbation theory. According to the microscopic Raman theory,[31,32] a first-order Raman scattering involves three processes, as shown in Figure 3a: (1) the electrons are stimulated from an initial ground state i to an intermediate state m by creating an electron−hole pair; (2) the electron−hole pair is scattered by a phonon into another intermediate state m'; and (3) the electron and hole recombine together to emit a photon and the system relaxes to the final state f.[31,32] Accordingly, the Raman intensity of a phonon as a function of the excitation energy can be described by[8,32]

$$I(E)_{\text{Raman}} \propto \left| \sum_{\mathbf{m},\mathbf{m}'} \frac{\langle \mathbf{f}|\mathbf{H}_{\text{light}}|\mathbf{m}'\rangle\langle \mathbf{m}'|\mathbf{H}_{\text{el-ph}}|\mathbf{m}\rangle\langle \mathbf{m}|\mathbf{H}_{\text{light}}|\mathbf{i}\rangle}{(E_\lambda - \Delta E_{\mathbf{m}i} - i\gamma_{\mathbf{m}})(E_\lambda - \Delta E_{\mathbf{m}'\mathbf{i}} - \hbar\omega - i\gamma_{\mathbf{m}'})} \right|^2 \quad (1)$$

where H_{light} and $H_{\text{el-ph}}$ are the electron−photon coupling and electron−phonon coupling Hamiltonians, respectively. γ_m and $\gamma_{m'}$ are the damping terms reflecting the finite lifetime of the intermediate states m and m'. E_λ and $\hbar\omega$ are the excitation photon energy and phonon energy, respectively. ΔE_{mi} and $\Delta E_{m'i}$ are the energy gaps between the initial ground state i and the intermediate states m and m'.[8,32]

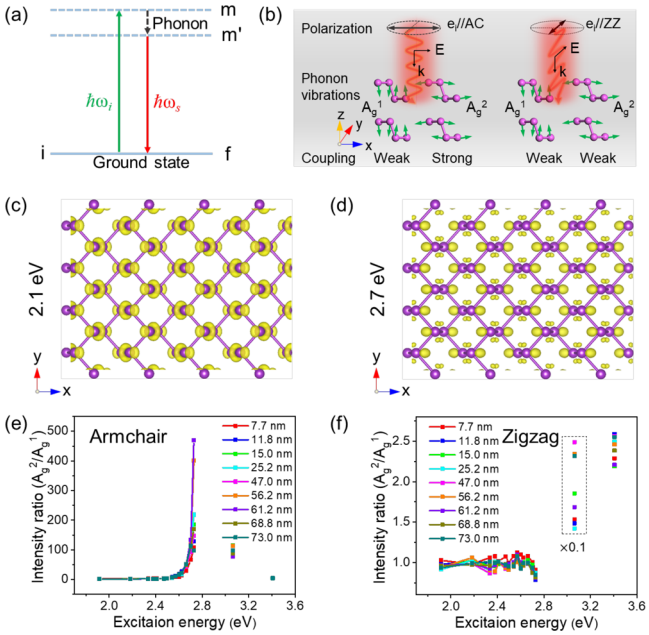

Figure 3. Symmetry-dependent electron−phonon coupling for the A_g phonons in BP. (a) Energy-level diagram for a Stokes Raman scattering process. (b) Schematic illustration of the match (orthogonality) of the A_g phonons vibration patterns with respect to the laser polarizations. (c and d) Calculated anisotropic electronic charge distributions of conduction states at two typical energies (c) 2.1 and (d) 2.7 eV above the valence band maximum of bulk BP. x and y in c and d denote the AC and ZZ crystalline orientations of BP structure. (e and f) Evolution of the Raman intensity ratio (A_g^2/A_g^1) along (e) the AC and (f) the ZZ directions as a function of the excitation energies for BP samples with the thicknesses of 7.7, 11.8, 15.0, 25.2, 47.0, 56.2, 61.2, 68.8, and 73.0 nm. Intensity ratios at 3.06 eV were multiplied by a factor of 0.1.

The distinct REPs for the A_g^1 and A_g^2 phonons with a laser polarization aligned along the same crystalline orientation can be understood by considering the symmetries of the corresponding excited states and the lattice vibrations of phonon modes in BP. Let us first discuss the REPs for the A_g^1 and A_g^2 phonons along the AC direction. In both cases, the BP sample was stimulated with P//AC and the allowed optical transitions between states i and m are equal for both A_g phonons, suggesting the first term in the numerator of eq 1 describing the electron−photon couplings is similar for the A_g^1 and A_g^2 phonons. Thereafter, the excited electrons will interact with the A_g^1 and A_g^2 phonons. Previous investigation has demonstrated that symmetry match between the phonons and the excitonic states in monolayer MoS_2 is vital to the exciton−phonon coupling.[5] Here, in our case, the A_g^1 and A_g^2 phonons possess similar phonon symmetry, and both of them involve coupled in-plane vibration and out-of-plane vibration.[33,34] However, the A_g^2 phonon has a larger vibration component along the AC direction, which matches the direction of the incident polarization (Figure 3b). As a result, the A_g^2 phonon couples more significantly with the electronic transition dipole allowed along in-plane AC direction, whereas for the A_g^1 phonon, the phosphorus atoms mainly vibrate along out-of-plane direction (z axis), and thus, it does not couple efficiently with the same electronic transition dipole. It follows that the A_g^2 phonon has a larger electron−phonon coupling term (the

DOI: 10.1021/jacs.9b07974
J. Am. Chem. Soc. 2019, 141, 18994−19001

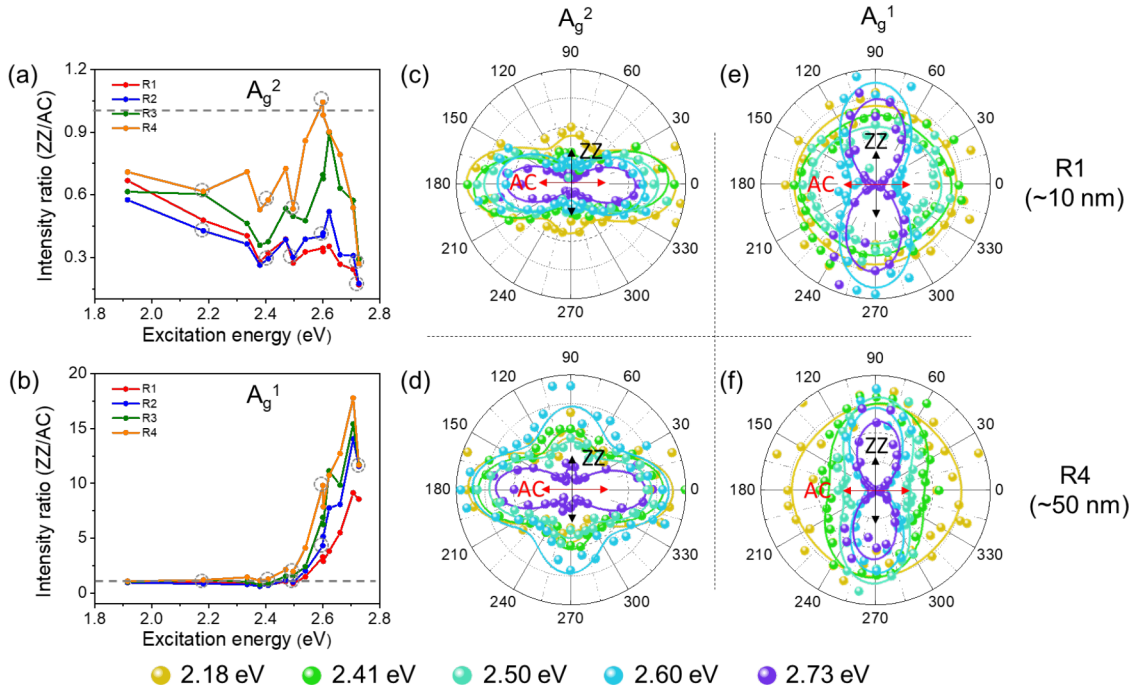

Figure 4. Comparison of the resonance effect of the A_g phonons for P//AC and P//ZZ and the corresponding anisotropic Raman intensities. (a and b) Evolution of the Raman intensity ratio of A_g^2 (a) and A_g^1 (b) modes between the ZZ and the AC directions (I_{ZZ}/I_{AC}) for four BP samples R1−R4. Horizontal dashed lines in a and b indicate $I_{ZZ}/I_{AC} = 1$. (c, d, e, and f) Polar plots of the angle-dependent Raman intensities of A_g^2 (c and d) and A_g^1 (e and f) modes for the BP sample R1 (~10 nm) (c and e) and R4 (~50 nm) (d and f) with excitation energies of 2.73, 2.60, 2.50, 2.41, and 2.18 eV (marked by dashed circles in a and b). Here 0° (90°) corresponds to the AC (ZZ) direction of BP.

second term in the numerator of eq 1) compared to the A_g^1 phonon along the AC direction.

This fact can also be understood by considering the match between the vibration patterns of A_g phonons and the symmetry of the electronic wave function of BP. According to the previous reports, the wave functions for bright excitons for single- and few-layer BP show anisotropic spatial distributions.[13,15] Specifically, these excitons form striped patterns and are mainly extended along the AC direction.[13,15] In our experiment, the thicknesses of BP samples range from several nanometers to 100 nm, and they are closer to bulk BP. Thus, we calculated the electronic wave functions of the excited states (conduction states) of bulk BP at different energies. They typically have anisotropic spatial electron distributions primarily extended along the AC direction, as illustrated in Figure 3c and 3d. Consequently, the movements of the phosphorus atoms along the AC direction of the A_g^2 phonon modulate the electronic cloud, which gives rise to stronger electron−phonon coupling in BP.[5] From the classical perspective of Raman scattering, since the phosphorus atoms in the A_g^2 phonon mode mainly vibrate along the AC direction, when excited by the laser polarized along the AC direction, the electric field of the applied incident electromagnetic wave would facilitate the atomic vibrations of the A_g^2 mode. In this scenario, one can expect larger electric dipole polarizability with stronger Raman intensity.

Moreover, the optical transition probability between states ***i*** and ***m*** of BP, determined by the electron−photon matrix element $\langle \mathbf{m}|\mathbf{H}_{light}|\mathbf{i}\rangle$, has been confirmed to be much larger for P//AC than for P//ZZ in the visible region.[13,17−19] The preferred optical transition along the AC direction and relatively larger electron−phonon coupling lead to the strongest resonance effect of A_g^2//AC. As shown in Figure 2a, this conclusion still holds in the UV region, despite the fact that the Raman intensities of the A_g phonons under the excitation at 3.41 eV are rather weak along both crystalline orientations.

Similarly, neither the A_g^1 nor A_g^2 phonon couples efficiently with the electronic states for P//ZZ excitation (Figure 3b) due to the near orthogonality of their vibration patterns with respect to the electronic transition dipole along the ZZ direction, which suggests relatively weak electron−phonon interaction. Moreover, the electron−photon interaction with P//ZZ is also very weak in the visible region, as previously reported.[12,13,17−19] Consequently, the weak electron−photon coupling and electron−phonon coupling lead to small $\langle \mathbf{m}|\mathbf{H}_{light}|\mathbf{i}\rangle$ and $\langle \mathbf{m}'|\mathbf{H}_{el-ph}|\mathbf{m}\rangle$ matrix elements, thus explaining the generally weak resonance effect for the A_g^1 and A_g^2 phonons when P//ZZ.

To compare the relative strengths of electron−phonon coupling for the A_g^1 and A_g^2 phonons in BP, we calculated their intensity ratios (A_g^2/A_g^1) as a function of the excitation energy (Figure 3e and 3f). Since both phonons were excited by the same excitation energy and laser polarization, the contributions of the electron−photon coupling and the interference effect to their REPs are nearly identical (here we neglect the small energy difference of these two phonons). Therefore, the intensity ratio A_g^2/A_g^1 reflects the relative strength of electron−phonon coupling term. As illustrated in Figure 3e, the electron−phonon coupling of A_g^2//AC is much larger than that of A_g^1 //AC in the visible and UV region, by 1 order of magnitude when the excitation energy is between 2.57 and 2.73 eV. This result is in accordance with our analysis based on quantum perturbation theory. In contrast, the electron−phonon couplings for A_g^1//ZZ and A_g^2//ZZ are practically the same in the visible region, as attested by the fact that the

DOI: 10.1021/jacs.9b07974
J. Am. Chem. Soc. 2019, 141, 18994−19001

intensity ratio of A_g^2 and A_g^1 remains to be 1 (Figure 3f). However, it becomes larger than 1 in the UV region, indicating a slightly larger electron−phonon coupling term for the A_g^2 phonon. This unusual effect can be understood by comparing the atomic vibrations of these two phonons with respect to the electronic wave function of BP with the excitation polarization along the ZZ direction. According to previous studies,[13,17] BP is almost transparent to the visible light polarized along the ZZ direction but starts to absorb in the UV region.

Compared to the out-of-plane A_g^1 phonon, the in-plane A_g^2 phonon tends to couple a little bit more strongly with the excited electronic states for the light polarization along the ZZ direction, even though both couplings are not as efficient as that of the A_g^2 phonon along the AC direction. Strong absorption in the UV region will also help to enhance the electron−phonon coupling of the A_g^2 mode, subsequently giving rise to larger intensity.

As shown in Figure 3e and 3f, we also compared the relative strength of intrinsic electron−phonon coupling for the A_g^1 and A_g^2 phonons in BP sample with various thicknesses (7.7 −73 nm). They have a similar trend within the excitation window. We believe that this conclusion still holds for even thicker BP sample, because their electronic structures and electron−phonon couplings remain similar to bulk BP. However, few-layer BP has distinct layer-dependent electronic structure, and thus might show different electron−phonon couplings as the case here. We think it will be very interesting and worth future investigation.

Nevertheless, it is more challenging to obtain few-layer BP samples by exfoliation due to the sample instability. The investigation on few-layer BP is ongoing, and preliminary data do suggest different trends from the thick and bulk samples, and the trends are indeed layer dependent. The results of few-layer BP for both high-frequency intralayer modes (A_g^1 and A_g^2) and low-frequency interlayer modes will be discussed and published in follow-up works.

Physical Origin of the Intricate Raman Anisotropy in BP. The polarized Raman spectra of anisotropic crystals are usually used to identify their crystalline orientations. Previous reports show that the angle-dependent polarized Raman intensity of A_g^2 can be used to identify the crystalline orientations of BP, based on the direction of the main axis of intensity polar plots.[24,27] However, it was found to be controversial among different groups whether the main axis of the intensity polar plots for A_g^2 is along the AC or ZZ direction.[19,22,23,25] Thereafter, the intricate anisotropic Raman intensity of BP was also found dependent on the excitation wavelength and sample thickness. The mechanism for this phenomenon was in disputation.[19,22,23,25]

In order to investigate the physical origin of the complex Raman anisotropy of BP and clarify the conclusion of identifying its crystalline orientations using the angle-dependent Raman method, we compared the REPs of the same A_g phonon with the laser polarization along two crystalline orientations. The Raman intensity ratios in these two cases (I_{ZZ}/I_{AC}) for the A_g phonons in four BP samples (R1−R4) are plotted in Figure 4a and 4b. Their thicknesses increase from R1 (∼10 nm) to R4 (∼50 nm). I_{ZZ}/I_{AC} is a key parameter to determine the pattern of the angle-dependent Raman intensity polar plots of the A_g phonons. We can see from Figure 4a that the excitation-energy-dependent I_{ZZ}/I_{AC} of A_g^2 is always below 1 for thin BP sample R1 (∼10 nm), which means the main axis of its angle-dependent Raman intensity of A_g^2 mode should always be along the AC direction.

To further confirm this fact, we performed the angle-dependent Raman measurements. As shown in Figure 4c, the polar plots of the angle-dependent Raman intensity of A_g^2 for sample R1 indeed always show the main axis along the AC direction under excitation energies of 2.18, 2.41, 2.50, 2.60, and 2.73 eV. This result is also consistent with our previous statement that both the electron−photon coupling and the electron−phonon coupling for the A_g^2 phonon are stronger for P//AC than for P//ZZ, which gives rise to the apparently stronger Raman intensity when P//AC. Therefore, we clarify here that under visible excitation energies, the polar plots of intrinsic angle-dependent polarized Raman intensity of A_g^2 show the main axis along the AC direction of BP. However, as the thickness of BP increases, the extrinsic interference effect might become rather significant under certain excitation energie (Figures S4c−f), and its contribution might be comparable to the intrinsic resonance effect. The main axis of the Raman intensity polar plot might flip over from the AC to the ZZ direction (Figure S6a) due to stronger interference effect along the ZZ direction. For instance, I_{ZZ}/I_{AC} for the 50 nm thick R4 sample is below 1 under most excitation energies, suggesting that the main axes of the angle-dependent Raman intensities of A_g^2 in this sample should be along the AC direction. As shown in Figure 4d, the measured Raman intensity polar plots of A_g^2 for this sample R4 indeed show the main axes along the AC direction under most excitation energies, such as 2.18, 2.41, 2.50, and 2.73 eV. However, when it is excited at 2.60 eV, due to large interference effect (Figure S5a) along the ZZ direction, I_{ZZ}/I_{AC} for A_g^2 mode shows a maximum with a value slightly above 1 (Figure 4a). As a result, the Raman intensity of A_g^2//AC is almost at the same level as that of A_g^2//ZZ, leading to the remarkable secondary peak in the intensity polar plot (Figure 4d), which makes it difficult to identify the crystalline orientation through the angle-dependent Raman intensity in this case.

As discussed above, the A_g^1 mode is mainly associated with out-of-plane atomic vibrations, and it does not show notable preference for coupling with the electronic states excited for P//AC or P//ZZ. Consequently, both A_g^1//ZZ and A_g^1//AC show a relatively weak resonance effect (Figure 2a) compared with that of A_g^2//AC. Therefore, it really depends on the specific excitation energy whether the resonance effect of A_g^1 mode is stronger along the AC or ZZ direction. As shown in Figure 2a, its resonance effect is comparable along the AC and ZZ directions for the excitation energies below 2.50 eV. Consequently, I_{ZZ}/I_{AC} fluctuates around 1 (Figure 4b), leading to the apparent absence of anisotropy in the intensity polar plots of the A_g^1 mode (round shape polar plots are seen in Figure 4e and 4f). In contrast, when the excitation energy exceeds 2.57 eV, the A_g^1 mode along the AC direction is gradually off-resonance, whereas it still shows considerable resonance along the ZZ direction (Figure 2a). Accordingly, I_{ZZ}/I_{AC} for the A_g^1 mode is significantly larger than 1, and the intensity polar plots display typical "8"-like shapes with the main axes along the ZZ direction (Figure 4b, 4e, and 4f). We also checked I_{ZZ}/I_{AC} for the A_g^1 phonon of BP samples with different thicknesses and found that it is always much larger than 1 for an excitation energy above 2.57 eV, regardless of the thickness of BP (Figure S6b). Although the interference effect contributes to the Raman intensity when the thickness of BP increases, the presence of a stronger interference effect along

DOI: 10.1021/jacs.9b07974
J. Am. Chem. Soc. 2019, 141, 18994−19001

the ZZ direction would widen the intensity gap between A_g^1//ZZ and A_g^1//AC. This result suggests that the angle-dependent Raman intensity of the A_g^1 phonon with the excitation energy between 2.60 and 2.73 eV can be used as an unambiguously reliable method to identify the crystalline orientations of BP. We randomly chose three excitation energies in this range to measure the angle-dependent Raman signals of BP samples with different thicknesses (8.4−103.3 nm); as listed in Table S1, the main axes of all of the polar plots for the A_g^1 phonon are along BP's ZZ direction.

CONCLUSION

In summary, we systematically investigated the electron−phonon coupling of BP using polarization-selective resonance Raman spectroscopy with the excitation energies covering the visible and UV regimes. For the in-plane A_g^2 mode of BP, polarization parallel to the AC direction (A_g^2//AC) exhibits strong resonance enhancement across visible wavelengths because the vibration pattern of this mode matches with the symmetry of the corresponding excited state. In contrast, polarization parallel to the ZZ direction (A_g^2//ZZ) reveals dramatically weaker electron−phonon coupling due to the orthogonality of its vibration pattern with respect to the related excited states. Similarly, we observe comparatively weak electron−phonon coupling for the out-of-plane A_g^1 mode (A_g^1//AC and A_g^1//ZZ) due to symmetry considerations. These results directly demonstrate symmetry-dependent electron−phonon coupling and can be understood by quantum perturbation theory considering the match between the phonon vibration pattern and the symmetry of the related excited states in BP. Further analysis of electron−phonon coupling allowed us to resolve the existing controversies on Raman identification of the crystal orientation in BP and the physical origin of intricate Raman anisotropy in anisotropic crystals. Our investigation opens an avenue for future exploration of the intricate polarized Raman scattering and electron−photon and electron−phonon couplings in other low-symmetry 2D materials.

ASSOCIATED CONTENT

Supporting Information

The Supporting Information is available free of charge on the ACS Publications website at DOI: 10.1021/jacs.9b07974.

Identifying the crystalline orientations of BP using angle-dependent Raman frequency; polarization and excitation-energy-dependent Raman spectra of BP; contribution of the optical interference enhancement to the resonance Raman excitation profiles of the A_g modes in BP; thickness-dependent Raman intensity ratio (I_{ZZ}/I_{AC}) of the A_g modes as a function of the excitation energies; thickness-dependent intensity polar plots of the A_g^1 mode under the excitation energy between 2.60 and 2.73 eV; density functional theory (DFT) calculations of the resonance Raman profiles (PDF)

AUTHOR INFORMATION

Corresponding Authors

*E-mail: liangl1@ornl.gov.
*E-mail: xiling@bu.edu.
*E-mail: jingkong@mit.edu.

ORCID

Nannan Mao: 0000-0003-3522-5341
Xingzhi Wang: 0000-0002-0929-854X
Yuxuan Lin: 0000-0003-0638-2620
Bobby G. Sumpter: 0000-0001-6341-0355
Qingqing Ji: 0000-0001-5526-3746
Tomás Palacios: 0000-0002-2190-563X
Shengxi Huang: 0000-0002-3618-9074
Vincent Meunier: 0000-0002-7013-179X
William A. Tisdale: 0000-0002-6615-5342
Liangbo Liang: 0000-0003-1199-0049
Xi Ling: 0000-0003-3462-9088
Jing Kong: 0000-0003-0551-1208

Author Contributions

‖N.M. and X.W. contributed equally to this work.

Notes

The authors declare no competing financial interest.

ACKNOWLEDGMENTS

N.M. and J.K. acknowledge the National Science Foundation grant 2DARE (EFRI-1542815) and DMR-1507806 for financial support. X.W. and X.L. are thankful for the funding support from Boston University. Part of this research (theoretical calculations) used resources at the Center for Nanophase Materials Sciences, which is a DOE Office of Science User Facility. Q.J. acknowledges support by the STC Center for Integrated Quantum Materials, NSF Grant No. DMR-1231319. Y.L. and T.P. acknowledge the partial support of the STC Center for Integrated Quantum Materials, NSF Grant No. DMR 1231319, and the U.S. Army Research Office through the MIT Institute for Soldier Nanotechnologies, under Award No. W911NF-18-2-0048. W.A.T. acknowledges support from the Alfred P. Sloan Foundation and the Camille & Henry Dreyfus Foundation. The authors also thank D. Tuschel, Dr. F. Adar, and Dr. B. A. O'Donnell from Horiba Co. and Dr. L. Lin and M. Wetherington from The Pennsylvania State University for the help of UV Raman experiments.

REFERENCES

(1) Martin, R. M.; Falicov, L. M. In *Light Scattering in Solids*; Cardona, M., Ed.; Springer Berlin Heidelberg: Berlin, Heidelberg, 1975; p 79.

(2) Eliel, G. S. N.; Moutinho, M. V. O.; Gadelha, A. C.; Righi, A.; Campos, L. C.; Ribeiro, H. B.; Chiu, P.-W.; Watanabe, K.; Taniguchi, T.; Puech, P.; Paillet, M.; Michel, T.; Venezuela, P.; Pimenta, M. A. Intralayer and Interlayer Electron−Phonon Interactions in Twisted Graphene Heterostructures. *Nat. Commun.* **2018**, *9*, 1221.

(3) Soubelet, P.; Bruchhausen, A. E.; Fainstein, A.; Nogajewski, K.; Faugeras, C. Resonance Effects in the Raman Scattering of Monolayer and Few-Layer $MoSe_2$. *Phys. Rev. B: Condens. Matter Mater. Phys.* **2016**, *93*, 155407.

(4) del Corro, E.; Terrones, H.; Elias, A.; Fantini, C.; Feng, S.; Nguyen, M. A.; Mallouk, T. E.; Terrones, M.; Pimenta, M. A. Excited Excitonic States in 1L, 2L, 3L, and Bulk WSe_2 Observed by Resonant Raman Spectroscopy. *ACS Nano* **2014**, *8*, 9629.

(5) Carvalho, B. R.; Malard, L. M.; Alves, J. M.; Fantini, C.; Pimenta, M. A. Symmetry-Dependent Exciton-Phonon Coupling in 2D and Bulk MoS_2 Observed by Resonance Raman Scattering. *Phys. Rev. Lett.* **2015**, *114*, 136403.

(6) del Corro, E.; Botello-Méndez, A.; Gillet, Y.; Elias, A. L.; Terrones, H.; Feng, S.; Fantini, C.; Rhodes, D.; Pradhan, N.; Balicas, L.; Gonze, X.; Charlier, J. C.; Terrones, M.; Pimenta, M. A. Atypical Exciton−Phonon Interactions in WS_2 and WSe_2 Monolayers Revealed by Resonance Raman Spectroscopy. *Nano Lett.* **2016**, *16*, 2363.

DOI: 10.1021/jacs.9b07974
J. Am. Chem. Soc. 2019, 141, 18994−19001

(7) Wang, X.; Mao, N.; Luo, W.; Kitadai, H.; Ling, X. Anomalous Phonon Modes in Black Phosphorus Revealed by Resonant Raman Scattering. *J. Phys. Chem. Lett.* **2018**, *9*, 2830.
(8) Jorio, A.; Saito, R.; Dresselhaus, G.; Dresselhaus, M. S. In *Raman Spectroscopy in Graphene Related Systems*; Jorio, A., Saito, R., Dresselhaus, G., Dresselhaus, M. S., Eds.; Wiley-VCH, 2011; p 103.
(9) McDonnell, L. P.; Huang, C. C.; Cui, Q.; Hewak, D. W.; Smith, D. C. Probing Excitons, Trions, and Dark Excitons in Monolayer WS_2 Using Resonance Raman Spectroscopy. *Nano Lett.* **2018**, *18*, 1428.
(10) Sariciftci, N. S.; Heeger, A. J.; Krasevec, V.; Venturini, P.; Mihailovic, D.; Cao, Y.; Libert, J.; Brédas, J. L. Symmetry-Specific Electron-Phonon Coupling for Electronic States near the Fermi Energy of Metallic Polyaniline: Resonant Raman Scattering. *Synth. Met.* **1994**, *62*, 107.
(11) Li, L.; Yu, Y.; Ye, G. J.; Ge, Q.; Ou, X.; Wu, H.; Feng, D.; Chen, X. H.; Zhang, Y. Black Phosphorus Field-Effect Transistors. *Nat. Nanotechnol.* **2014**, *9*, 372.
(12) Yuan, H. T.; Liu, X. G.; Afshinmanesh, F.; Li, W.; Xu, G.; Sun, J.; Lian, B.; Curto, A. G.; Ye, G. J.; Hikita, Y.; Shen, Z. X.; Zhang, S. C.; Chen, X. H.; Brongersma, M.; Hwang, H. Y.; Cui, Y. Polarization-Sensitive Broadband Photodetector Using a Black Phosphorus Vertical P−N Junction. *Nat. Nanotechnol.* **2015**, *10*, 707.
(13) Tran, V.; Soklaski, R.; Liang, Y. F.; Yang, L. Layer-Controlled Band Gap and Anisotropic Excitons in Few-Layer Black Phosphorus. *Phys. Rev. B: Condens. Matter Mater. Phys.* **2014**, *89*, 235319.
(14) Zhang, S.; Yang, J.; Xu, R.; Wang, F.; Li, W.; Ghufran, M.; Zhang, Y.-W.; Yu, Z.; Zhang, G.; Qin, Q.; Lu, Y. Extraordinary Photoluminescence and Strong Temperature/Angle-Dependent Raman Responses in Few-Layer Phosphorene. *ACS Nano* **2014**, *8*, 9590.
(15) Wang, X.; Jones, A. M.; Seyler, K. L.; Tran, V.; Jia, Y.; Zhao, H.; Wang, H.; Yang, L.; Xu, X.; Xia, F. Highly Anisotropic and Robust Excitons in Monolayer Black Phosphorus. *Nat. Nanotechnol.* **2015**, *10*, 517.
(16) Yang, J.; Xu, R.; Pei, J.; Myint, Y. W.; Wang, F.; Wang, Z.; Zhang, S.; Yu, Z.; Lu, Y. Optical Tuning of Exciton and Trion Emissions in Monolayer Phosphorene. *Light: Sci. Appl.* **2015**, *4*, No. e312.
(17) Qiao, J.; Kong, X.; Hu, Z.-X.; Yang, F.; Ji, W. High-Mobility Transport Anisotropy and Linear Dichroism in Few-Layer Black Phosphorus. *Nat. Commun.* **2014**, *5*, 4475.
(18) Xia, F.; Wang, H.; Jia, Y. Rediscovering Black Phosphorus as an Anisotropic Layered Material for Optoelectronics and Electronics. *Nat. Commun.* **2014**, *5*, 4458.
(19) Ling, X.; Huang, S.; Hasdeo, E. H.; Liang, L.; Parkin, W. M.; Tatsumi, Y.; Nugraha, A. R.; Puretzky, A. A.; Das, P. M.; Sumpter, B. G.; Geohegan, D. B.; Kong, J.; Saito, R.; Drndic, M.; Meunier, V.; Dresselhaus, M. S. Anisotropic Electron-Photon and Electron-Phonon Interactions in Black Phosphorus. *Nano Lett.* **2016**, *16*, 2260.
(20) Luo, Z.; Maassen, J.; Deng, Y.; Du, Y.; Garrelts, R. P.; Lundstrom, M. S.; Ye, P. D.; Xu, X. Anisotropic in-Plane Thermal Conductivity Observed in Few-Layer Black Phosphorus. *Nat. Commun.* **2015**, *6*, 8572.
(21) Mao, N.; Tang, J.; Xie, L.; Wu, J.; Han, B.; Lin, J.; Deng, S.; Ji, W.; Xu, H.; Liu, K.; Tong, L.; Zhang, J. Optical Anisotropy of Black Phosphorus in the Visible Regime. *J. Am. Chem. Soc.* **2016**, *138*, 300.
(22) Kim, J.; Lee, J. U.; Lee, J.; Park, H. J.; Lee, Z.; Lee, C.; Cheong, H. Anomalous Polarization Dependence of Raman Scattering and Crystallographic Orientation of Black Phosphorus. *Nanoscale* **2015**, *7*, 18708.
(23) Ribeiro, H. B.; Pimenta, M. A.; de Matos, C. J.; Moreira, R. L.; Rodin, A. S.; Zapata, J. D.; de Souza, E. A.; Castro Neto, A. H. Unusual Angular Dependence of the Raman Response in Black Phosphorus. *ACS Nano* **2015**, *9*, 4270.
(24) Wu, J.; Mao, N.; Xie, L.; Xu, H.; Zhang, J. Identifying the Crystalline Orientation of Black Phosphorus Using Angle-Resolved Polarized Raman Spectroscopy. *Angew. Chem., Int. Ed.* **2015**, *54*, 2366.
(25) Mao, N.; Wu, J.; Han, B.; Lin, J.; Tong, L.; Zhang, J. Birefringence-Directed Raman Selection Rules in 2D Black Phosphorus Crystals. *Small* **2016**, *12*, 2627.
(26) Mao, N.; Zhang, S.; Wu, J.; Zhang, J.; Tong, L. Lattice Vibration and Raman Scattering in Anisotropic Black Phosphorus Crystals. *Small Methods* **2018**, *2*, 1700409.
(27) Lu, W.; Ma, X.; Fei, Z.; Zhou, J.; Zhang, Z.; Jin, C.; Zhang, Z. Probing the Anisotropic Behaviors of Black Phosphorus by Transmission Electron Microscopy, Angular-Dependent Raman Spectra, and Electronic Transport Measurements. *Appl. Phys. Lett.* **2015**, *107*, 021906.
(28) Ribeiro, H. B.; Pimenta, M. A.; de Matos, C. J. S. Raman Spectroscopy in Black Phosphorus. *J. Raman Spectrosc.* **2018**, *49*, 76.
(29) Wang, T.; Liu, J.; Xu, B.; Wang, R.; Yuan, P.; Han, M.; Xu, S.; Xie, Y.; Wu, Y.; Wang, X. Identifying the Crystalline Orientation of Black Phosphorus by Using Optothermal Raman Spectroscopy. *ChemPhysChem* **2017**, *18*, 2828.
(30) Liang, L.; Wang, J.; Lin, W.; Sumpter, B. G.; Meunier, V.; Pan, M. Electronic Bandgap and Edge Reconstruction in Phosphorene Materials. *Nano Lett.* **2014**, *14*, 6400.
(31) Loudon, R. Theory of the Resonance Raman Effect in Crystals. *J. Phys. (Paris)* **1965**, *26*, 677.
(32) Rousseau, D. L.; Friedman, J. M.; Williams, P. F. In *Raman Spectroscopy of Gases and Liquids*; Weber, A., Ed.; Springer Berlin Heidelberg: Berlin, Heidelberg, 1979; p 203.
(33) Ribeiro-Soares, J.; Almeida, R. M.; Cançado, L. G.; Dresselhaus, M. S.; Jorio, A. Group Theory for Structural Analysis and Lattice Vibrations in Phosphorene Systems. *Phys. Rev. B: Condens. Matter Mater. Phys.* **2015**, *91*, 205421.
(34) Cai, Y.; Ke, Q.; Zhang, G.; Feng, Y. P.; Shenoy, V. B.; Zhang, Y.-W. Giant Phononic Anisotropy and Unusual Anharmonicity of Phosphorene: Interlayer Coupling and Strain Engineering. *Adv. Funct. Mater.* **2015**, *25*, 2230.

DOI: 10.1021/jacs.9b07974
J. Am. Chem. Soc. 2019, 141, 18994−19001